AIMS Geosciences

AIMS Geosciences, 11(4): 907–922.
DOI: 10.3934/geosci.2025039
Received: 30 May 2025
Revised: 29 August 2025
Accepted: 15 September 2025
Published: 05 November 2025

https://www.aimspress.com/journal/geosciences

Research article

Ice content dependence of fluctuating basal forces in rock–ice avalanche: From numerical rotating drum tests

Zhibo Dong* and Zhiping Sun

College of Civil and Architectural Engineering, Liaoning University of Technology, Jinzhou City, 121000, China

* **Correspondence:** Email: dongzhibo@lnut.edu.cn; Tel: +86-176-4826-1906.

Abstract: In this study, we investigated ice content effects on basal force fluctuations in rock-ice avalanches using discrete element method (DEM) rotating drum simulations. Calibrated DEM parameters reproduced experimental benchmarks, enabling numerical tests across ice contents (0–100%). Our results demonstrated ice-driven phase segregation: Low-density ice particles migrate to flow fronts, while gravel accumulates in tails. Increasing ice content linearly reduced the mean basal force, extreme force, and force standard deviation, attributed to ice's friction reduction and lubrication effects. Statistical analysis revealed that basal force fluctuations followed the Generalized Pareto Distributions, with heavier tails under low ice content indicating heightened stochasticity. Normal and shear stress fluctuations exhibited power-law correlations with solid inertial stress, confirming that collisional interactions dominated force variability. Ice-mediated lubrication diminished interparticle locking, promoting collision-driven momentum transfer and altering rheological behavior. These findings elucidate mechanisms linking ice content to segregation and basal forces, offering theoretical insights for modeling rock-ice avalanche hazards.

Keywords: rock-ice avalanche; DEM; rotating drum; basal force; fluctuation

1. Introduction

Rock-ice avalanches refer to large-scale slope failures characterized by the involvement of ice during initiation or transport processes [1,2]. Such phenomena exhibit heightened sensitivity to climatic variations. In alpine and cryospheric environments, the destabilization of slopes, driven by

glacial retreat and permafrost thaw, frequently triggers rapid and voluminous mass movements. Recent decades have witnessed a marked rise in the frequency of these events within glaciated regions, a trend strongly correlated with global warming and intensified anthropogenic activities [3,4]. Historical records and empirical studies [5,6] highlight their catastrophic potential, attributed to both their massive scale and exceptional mobility. Notably, these dynamics often result in severe societal impacts, including significant loss of life and infrastructure damage [7,8].

Rock-ice avalanches demonstrate flow-like dynamics accompanied by progressive boundary erosion. This process amplifies their destructive capacity through substrate entrainment, as mobilized material integrates into the moving mass. Critical to understanding these dynamics is the basal interaction force, which governs both erosional intensity and flow mobility [9,10]. Establishing mechanistic erosion models capable of predicting substrate wear requires precise identification of the variables modulating basal forces. While prior research has explored basal force mechanics in dry granular flows and debris surges through experimental and field observations [11–15], rock-ice avalanches present unique challenges. Their transient nature and inherent unpredictability severely limit opportunities for direct field measurements across spatial or temporal dimensions. As a result, existing knowledge predominantly relies on post-event remote sensing analyses and localized source-area surveys. A critical knowledge gap persists: the physical quantification of key parameters regulating flow behavior and substrate interaction forces remains elusive.

The dynamic behavior of rock-ice avalanches involves intricate particle interactions that remain challenging to quantify [16]. Conventional experimental approaches often failed to eliminate interference from ice melt under ambient conditions, introducing uncertainties into outcome interpretations. Furthermore, during such experiments, data acquisition was confined to bulk-scale measurements, leaving granular-level interaction mechanisms unresolved. These limitations underscore the necessity of discrete element method (DEM) simulations, which enable systematic parameter adjustments in controlled environments to replicate flow dynamics and extract granular-scale mechanical insights.

We employed a DEM-based rotating drum apparatus to investigate how varying ice content influences basal force characteristics (normal and shear) in simulated rock-ice avalanches. The rotating drum design facilitates prolonged data acquisition at controlled flow velocities, capturing dynamic profiles of granular-ice mixtures over sustained observation periods. By leveraging this setup, high-resolution statistical analysis of basal interactions is achievable, offering mechanistic insights into ice-mediated flow dynamics. We aim to enhance our understanding of ice-rich mass flow behaviors, providing a theoretical foundation for modeling analogous geophysical hazards such as debris-laden landslides and glacial surges.

2. Methods

2.1. Configuration of DEM simulation

Contemporary physical modeling of rock-ice avalanches predominantly employs two experimental configurations: Inclined chute [1,2,16] and rotating drum tests [16–18]. While the drum's curved boundary geometry deviates from natural topographic conditions, its rotational mechanics provide critical advantages over chute systems for simulating phase-transition dynamics. The sustained centrifugal motion in drum experiments facilitates (1) continuous ice melting processes essential for

capturing solid-liquid interaction during flow state evolution, and (2) stable multiphase flow conditions, enabling quantitative analysis of ice content and meltwater ratio controls on rheological behavior. Recent drum-based investigations in references [17] and [18] have successfully characterized basal pressure regimes and mobility indices through triaxial force sensor. Nevertheless, inherent limitations persist in physical modeling approaches, including restricted capacity for micromechanical particle interaction analysis and substantial resource expenditures in experimental operations. Numerical simulations emerge as a potent complementary methodology, overcoming these constraints through DEM that enables granular-scale interaction quantification and time-efficient parametric studies. As shown in Figure 1, we establish a DEM-based drum model replicating the experimental configuration of reference [17], which features a 1.50 m outer diameter drum with 0.90 m inner diameter and 0.30 m width, incorporating a steel base, acrylic sidewalls, and triaxial transducers for normal/shear stress measurement at the flow-base interface. We focus on identifying the ice content (volume fraction of ice) affecting the fluctuating basal forces of rock–ice avalanche, and the ice contents are 0%, 20%, 40%, 60%, 80%, and 100%.

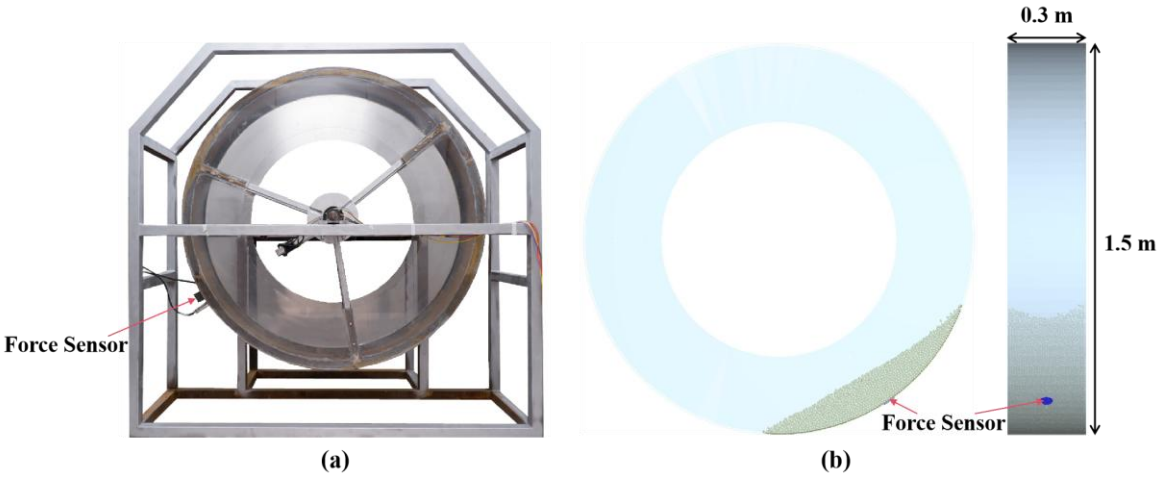

Figure 1. (a) Photo of rotating drum in references [17]. (b) The DEM model of a rotating drum.

2.2. DEM parameter calibration

Numerical simulations of rock-ice avalanches using the DEM necessitate a more sophisticated parameter calibration protocol compared to their purely rocky counterparts. The preliminary phase requires meticulous adjustment of both material properties (including density, Poisson's ratio, and shear modulus) and interaction coefficients (such as restitution, static friction, and rolling friction parameters) to ensure model fidelity. For material properties, ice and gravel parameters are extracted from validated material libraries (Table 1), ensuring consistency with established geomechanical standards.

Table 1. Physical parameters of materials in DEM.

Materials	Particle density (kg/m^3)	Poisson's ratio	Shear modulus (GPa)
Gravel	2550	0.25	1.6
Ice	917	0.30	1.54

For contact parameter calibration, the restitution coefficient exhibited statistically insignificant impact on simulation outcomes under quasi-static conditions where high-energy collisions are absent. This observation justifies the systematic retention of restitution coefficient = 0.5 throughout the calibration process to enhance computational efficiency while maintaining physical fidelity. As shown in Figure 2, experimental measurements by researchers [18] established reference benchmarks for validation: (1) Repose angles of 34.0°, 23.5°, and 11.7° for pure gravel assembly, ice-gravel mixture (50% ice by volume), and pure ice system at −10°C, respectively; (2) bulk dynamic friction coefficient of 20.2° under φ_i = 40% ice content in rotating drum tests. DEM simulations incorporating calibrated interparticle contact parameters from Table 2 yields repose angles of 37.5°, 24.3°, and 13.6° for the respective pure gravel, mixed-phase (50% ice), and pure ice configurations. The rotating drum simulations under φi = 40% ice content produces a repose angle of 20.1°, demonstrating remarkable consistency with experimental measurements. Experimental benchmarks from researchers [18] utilize angular gravel and cubic ice particles, whereas DEM simulations adopt spherical approximations for computational efficiency. The friction parameters in Table 2 are calibrated to compensate for morphology-induced effects, ensuring consistent rheological behavior across scales. This parametric validation confirms the physical rationality of the DEM microparameters, particularly regarding ice-rock interaction modeling. The discrepancy between numerical and experimental results falls within acceptable error margins for granular flow simulations, as established in prior studies.

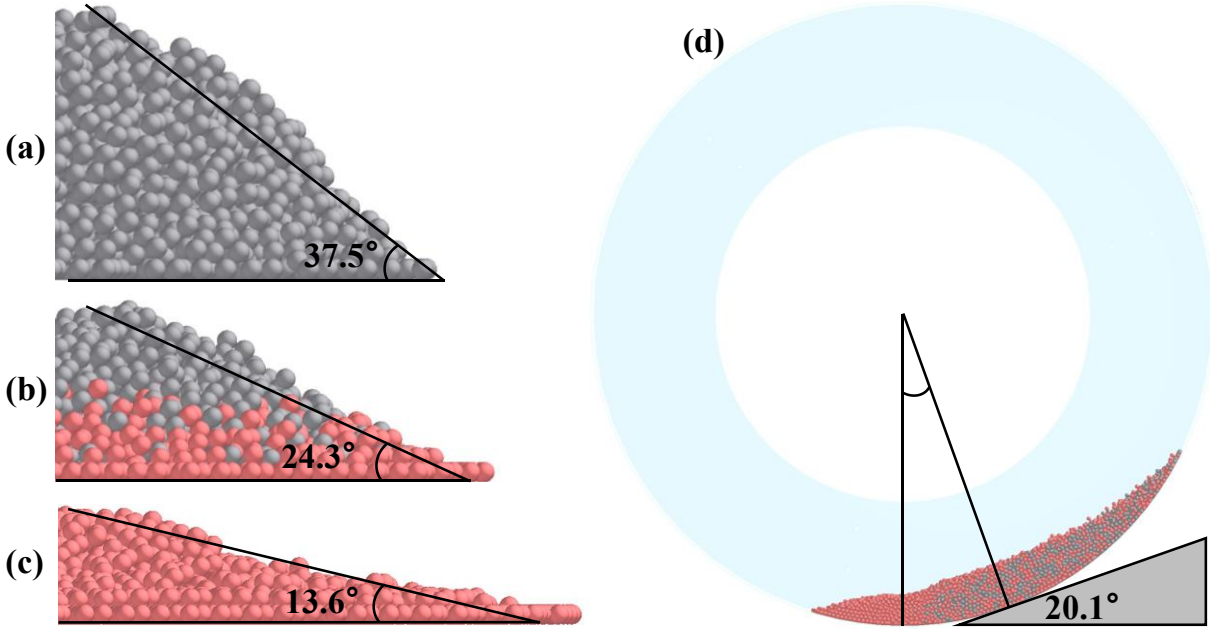

Figure 2. In the Discrete Element Method (DEM) model for angle of repose analysis, gravel particles are represented by dark gray spheres, while ice particles are depicted in light red. The simulation includes four scenarios: (a) Pure gravel; (b) mixed-phase system with 50% ice content; (c) pure ice; and (d) drum test for angle of repose measurement with ice volume fraction φ_i = 40%.

Table 2. Contact parameters between materials in DEM.

Contact group	Restitution coefficient	Static friction coefficient	Rolling friction coefficient
Gravel-Gravel	0.50	0.60	0.10
Gravel-Ice	0.50	0.27	0.05
Ice-Ice	0.50	0.11	0.01

3. Results and discussions

3.1. Visual description of the flows

Figure 3 illustrates the top view of rock-ice avalanche dynamics within a rotating drum under varying ice content conditions. As depicted in Figure 3, the rock-ice binary granular flow exhibits pronounced segregation during drum rotation: ice particles preferentially accumulate at the flow front, while gravel particles settle dominantly in the trailing region. This bidirectional phase separation arises from the interplay of differential density and frictional properties between the two phases [19,20]. Ice particles (lower density ρ_{ice} = 917 kg/m³) migrate upward through buoyancy-driven percolation as they are displaced by sinking gravel particles (ρ_{rock} = 2550 kg/m³). Furthermore, the lower interparticle friction of ice (μ_{ice} = 0.11–0.27 vs. μ_{gravel} = 0.27–0.60) enhances their mobility over rock-dominated zones, accelerating frontal accumulation [21].

Building on these observations, experimental [17] and numerical analyses [20–23] provide deeper mechanistic insights. They reveal that ice particles, characterized by lower density and reduced frictional coefficients, exhibit preferential migration toward the flow front through buoyancy-driven mechanism. Gravel particles undergo gravitational settling driven by density contrast, while their higher friction coefficients amplify collisional dissipation. This collectively promotes tailward concentration, delaying gravel transport relative to the flow front. Importantly, the resultant spatial heterogeneity in phase distribution dynamically regulates energy dissipation pathways; ice-dominated zones at flow fronts exhibit lower collisional damping due to reduced restitution coefficients and friction-mediated sliding contacts, conserving kinetic energy despite higher collision frequency, whereas rock-rich domains enhance energy dissipation via frictional interactions [20,24].

To summarize the dominant segregation mechanisms: Density differences dominate vertical percolation, driving ice upward and gravel downward [21]. However, in the context of rotating drum flows, where the flow direction is constrained, the axial (front-back) segregation is modulated by friction hierarchy. Specifically, low-friction ice slides efficiently over gravel-dominated zones toward the drum's leading edge, while high-friction gravel resists forward transport due to enhanced collisional dissipation (Figure 3). A critical point to note is that this lateral mobility operates orthogonally to vertical density stratification, avoiding mechanistic conflict. Such self-reinforcing segregation patterns are particularly pronounced in shear-dominated flow regimes, where velocity gradients amplify the differential mobility of ice and rock phases, establishing a positive feedback loop between phase separation and flow acceleration. Overall, this mechanistic understanding underscores the critical and complementary role of density-driven and friction-driven segregation in governing the hypermobility and erosive potential of ice-rock avalanches.

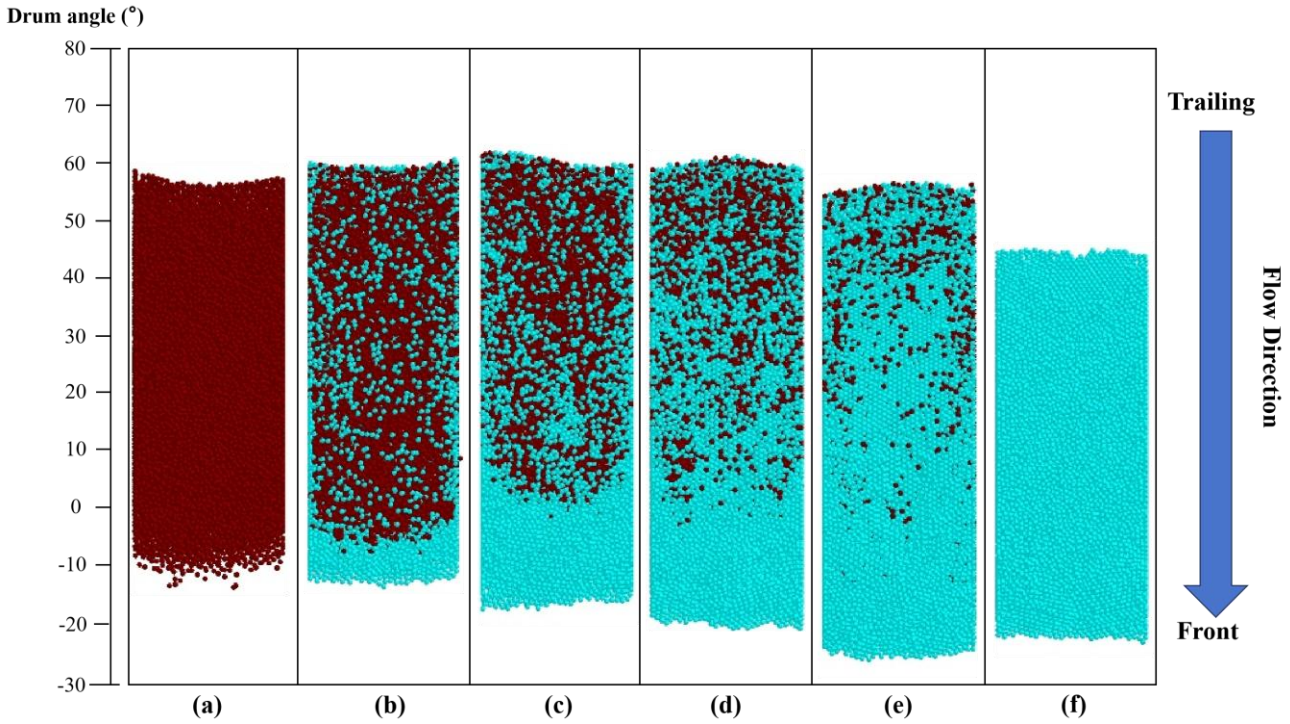

Figure 3. Top views of rock-ice avalanches with different ice content (φ_i): (a) φ_i = 0%; (b) φ_i =20%; (c) φ_i = 40%; (d) φ_i = 60%; (e) φ_i = 80%; and (f) φ_i = 100%. The gravel particles are represented by brown spheres, while ice particles are depicted in light blue. The left-hand scale indicates the location where the granular mixture flow in the rotating drum.

3.2. Profiles of normal and shear forces

The basal normal and shear forces are quantified through a 4 cm-diameter force plate integrated with the rotating drum substrate (Figure 1), the force plate shares identical steel material composition and surface properties with the drum base, ensuring material homogeneity and representative flow dynamics. Granular flow kinematics demonstrate pronounced sensitivity to boundary roughness, with rough interfaces suppressing coherent crystalline formations observed in smooth boundary conditions. In this experimental configuration, rock-ice avalanches traverse drum boundaries prior to interacting with the force plate. Fortunately, the force plate exhibits a comparatively smaller dimension relative to the 30 cm-diameter rotating drum base while sharing identical material composition with the other section of drum base. Hence, flow dynamics measured by the plate should be representative of those developed over drum base.

For all simulations, steady flow of rock-ice avalanches developed after several rotations of the drum. Typical force measurements recorded during a single traverse across the force plate reveal the influence of ice concentration (φ_i) on flow dynamics, including spatial distribution and fluctuation intensity (Figure 4). The leading edge of the flow exhibits a progressive downstream displacement (toward lower angular positions on the drum) with elevated φ_i. Maximum upstream positioning of the flow front occurs either in pure granular flows or mixtures with φ_i = 20% (Figure 4a, b). The ice content exhibits a negative correlation with flow resistance between rock-ice avalanches and the base of rotating drum. Moreover, experimental studies demonstrate that increased ice content reduces Coulomb frictional stress. This inverse relationship stems from two mechanisms: (1) Ice decrease

interparticle friction coefficients through their lower surface roughness compared to rock particles, reducing shear resistance at the flow boundary; and (2) Higher ice content promotes vertical segregation of ice particles toward free surfaces, creating internal lubricating layers that reduce system-wide frictional dissipation. This indirectly modifies stress transmission patterns to the base by enhancing collisional momentum transfer and minimizing force chain instabilities within the avalanche mass. Most flows exhibit comparable force distribution patterns characterized by lateral imbalance; a sharp surge to peak values immediately trailing the leading edge, followed by a progressive decline toward the tail. In contrast, ice-rich mixtures ($\varphi_i \geq 30\%$, Figure 4e) demonstrate enhanced symmetry, with temporally averaged peak forces centralized within the profile. Notably, oscillation amplitudes in high-frequency components diverge significantly across material compositions.

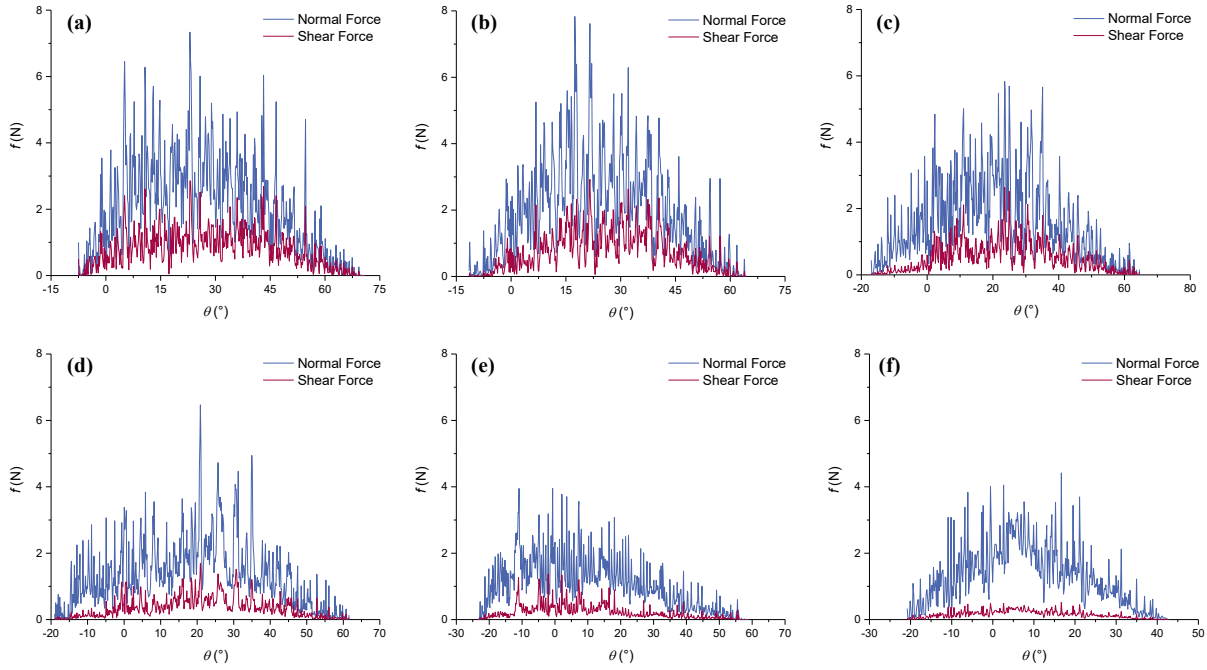

Figure 4. Profiles of normal and shear forces of rock-ice avalanches with different ice content (φ_i): (a) φ_i = 0%; (b) φ_i = 20%; (c) φ_i = 40%; (d) φ_i = 60%; (e) φ_i = 80%; and (f) φ_i = 100%.

The probability distribution characteristics of basal force in rock-ice avalanches can be quantitatively described using the Generalized Pareto Distribution (GPD). As illustrated in Figure 5, the horizontal axis represents the basal normal force (f_n) and shear stress (f_s) measured by a force plate under varying ice content conditions, while the vertical axis corresponds to the probability density values [GPD (f)]. Numerical simulations demonstrate that the statistical features of the basal force field conform to the mathematical formulation of the GPD. Its cumulative distribution function is expressed as:

$$GPD(f) = \left(\frac{1}{f_p}\right)\left(1 + k_p \frac{f - \theta_p}{f_p}\right)^{-1-\frac{1}{k_p}} \tag{1}$$

where k_p is the shape parameter that governs the tail behavior of the distribution; f_p is the scale parameter that characterizes the dispersion of stress distribution; and θ_p is the location parameter, representing the lower threshold of stress [25].

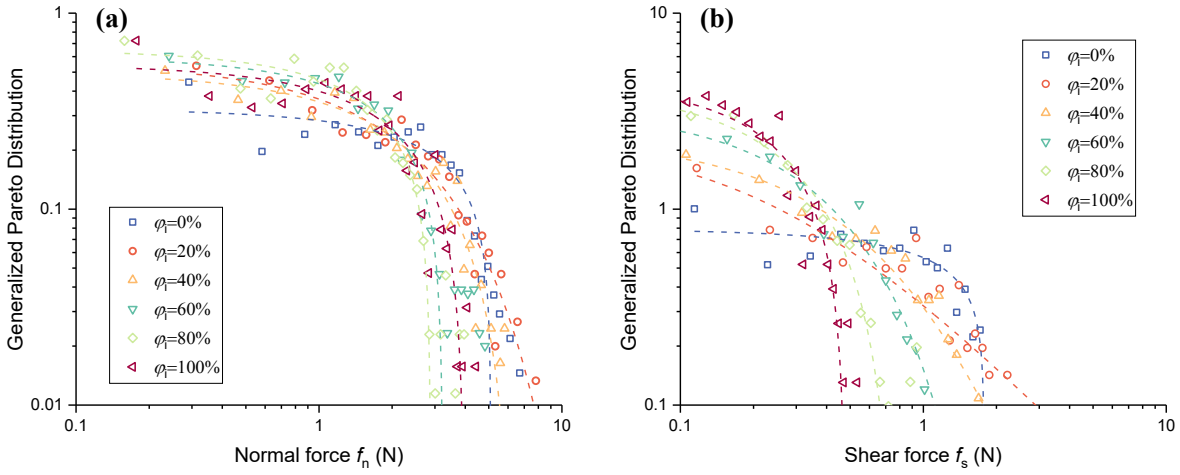

Figure 5. Distribution of probability density of basal normal and shear forces (scatter) and their generalized Pareto distribution (dotted line).

Table 3. The fitting parameters of the generalized Pareto distribution of basal force.

Run Number	Run Description	Fitting Parameters							
		f_p	k_p	θ_p	R^2	f_p	k_p	θ_p	R^2
1	φ_i = 0%	3.01	−0.61	0.03	0.87	1.26	0.71	3.32	0.89
2	φ_i = 20%	2.12	−0.11	0.39	0.95	19.48	3.65	5.07	0.87
3	φ_i = 40%	2.09	−0.32	0.11	0.94	0.53	0.23	0.08	0.97
4	φ_i = 60%	1.69	−0.53	0.07	0.96	0.34	−0.09	0.04	0.97
5	φ_i = 80%	1.55	−0.55	0.05	0.92	0.25	−0.31	0.02	0.98
6	φ_i = 100%	1.86	−0.48	0.07	0.83	0.22	−0.47	0.009	0.84

The experimental data of basal forces presented in Figure 5 exhibit a strong agreement with the Generalized Pareto Distribution (GPD) model. Table 3 summarizes the optimal GPD parameters (shape k_p, scale f_p, and location θ_p) across varying ice content conditions. A critical focus of the probability density analysis lies in the tail behavior of the distribution curves. Heavier tails (i.e., slower decay rate) indicate a higher probability of extreme basal force values, intensified force fluctuations, and enhanced erosive potential on the base. As visually demonstrated in Figure 5, reduced ice content correlates with elongated tails in the normal stress distributions. This phenomenon can be mechanistically attributed to three interdependent factors: (1) The ice-content-induced mass reduction of the granular mixture (ρ_s <

ρ_r), decreasing gravitational forcing; (2) gravel segregation toward the base (Figure 3) that enhances interparticle locking and bed shearing; and (3) ice's intrinsic friction reduction at particle contacts. While mass reduction contributes to force attenuation, DEM analysis confirms that friction reduction dominates the trend, as evidenced by the disproportionate force decrease relative to density changes (e.g., 100% ice reduces density by 64% but basal force by >80%).

3.3. Clinical trial registration

The basal forces for rock–ice avalanches in this study are statistically characterized through three key metrics [17,25]: Mean force ($\bar{f}$), extreme force ($f_{1\%}$), and the standard deviation of force (f_{sd}). Among these, $\bar{f}$ is a critical indicator of quasi-static flow loading, consistent with prior experimental frameworks for granular flows [26,27]. This parameter is operationally defined as the arithmetic mean of all force plate measurements over the entire duration of an avalanche event:

$$\bar{f} = \frac{1}{N}\sum_{i=1}^{N} f_i , \tag{2}$$

where N is the total number of force data points measured.

The temporal averaging method is a standardized metric for quantifying the central tendency of basal force in granular flow systems. To address the inherent limitations of this approach in capturing extreme loading events, a robust statistical framework is implemented, wherein the 99th percentile of force measurements, which is employed to mitigate stochastic interference from random variability. This percentile-based thresholding in extreme value theory, enables precise isolation of high-magnitude force transients while maintaining statistical rigor. Formally, the extreme force component is calculated as:

$$f_{1\%} = \frac{1}{N_{i\geq 99\%}} \sum f_i \geq f_{99\%} , \tag{3}$$

where $f_{99\%}$ is the 99th percentile of the cumulative force distribution, and $N_{i\geq 99\%}$ denotes the total number of stress measurements exceeding 99% of the measured values.

The temporal variability of basal stress amplitudes, quantified through standard deviation (f_{sd}, Equation 4), is a robust metric for characterizing dynamic force fluctuations in granular flow systems. This statistical parameter effectively captures the stochastic nature of interparticle collisions and transient force chain formations [14,18].

$$f_{sd} = \sqrt{\frac{1}{N}\sum_{i=1}^{N}(f_i - \bar{f}_i)} . \tag{4}$$

The fluctuation characteristics of basal forces (including normal and shear components) in rock-ice avalanches exhibit a significant dependency on ice content. Quantitative analysis demonstrates that key fluctuation indices, namely the time-averaged basal force, extreme basal force magnitude, and standard deviation of basal forces, all display linear decreasing trends with increasing ice fraction (Figure 6a-c). This phenomenon can be mechanistically attributed to the ice-content-induced mass

reduction of the granular mixture. As evidenced by previous granular flow studies [14,25,26], the amplitude of stress fluctuations shows strong positive correlations with total mass or bulk volume of particulate systems, a relationship that aligns with our experimental observations under controlled boundary conditions.

The extreme basal forces predominantly originate from discrete particle-bed collisions, which generate impulsive stress peaks due to high-energy impacts. While collisional interactions are the exclusive source of force fluctuations in our DEM framework, this is evidenced by the robust correlation between extreme force and fluctuation intensity (Figure 6d). The observed coupling between these two metrics strongly suggests that the basal force fluctuations in rock-ice avalanches are primarily governed by stochastic particle impact events rather than sustained frictional contacts. This mechanical behavior reflects ice-mediated modifications of conventional granular flow dynamics, where reduced interparticle friction promotes a shift toward collision-dominated momentum transfer. While this shares similarities with dry granular rheology, the observed power-law stress scaling (Figure 7) suggests potential distinctions requiring further investigation across broader parametric ranges.

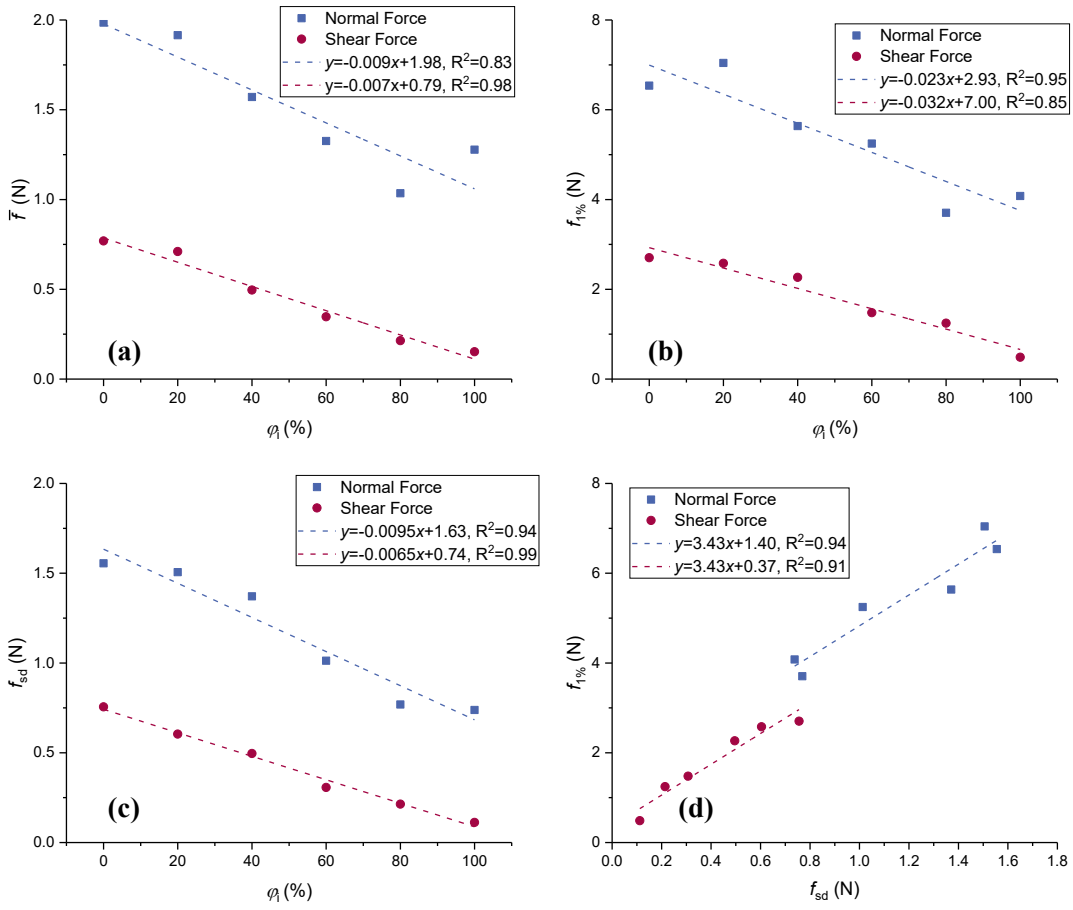

Figure 6. The relationship between (a) mean force $\bar{f}$ and ice content φ_i; (b) extreme force $f_{1\%}$ and ice content φ_i; (c) standard deviation f_{sd} of basal force and ice content φ_i; and (d) extreme force $f_{1\%}$ and standard deviation f_{sd} of basal force.

3.4. The relationship between basal stress fluctuations and flow dynamics

Solid inertial stress (T) is a constitutive parameter that quantifies the collisional interactions within granular flows, defined as a function of flow depth, grain size, shear rate, and solid volume fraction. Following Bagnold's scaling framework [28] and extended for geophysical flows [13,29], T can be expressed as:

$$T = \upsilon_s \rho_s \dot{\gamma}^2 d^2 \tag{5}$$

where ρ_s is the weighted average density of gravel (ρ_g) and ice (ρ_i) in a rock-ice avalanche, and $\rho_s = \varphi_i\rho_i + (1-\varphi_i)\rho_g$ is the shear rate ($=v/h$, v and h are the velocity and the flow depth of the rock-ice avalanche). d is the particle size. Figure 7 shows the correlations between f_{sd} and T of the rock-ice avalanche under different ice content conditions. The standard deviations of basal normal and shear forces exhibit distinct positive power-law correlations with the inertial stress (normal force: $R^2 = 0.68$; shear force: $R^2 = 0.92$), with the shear force demonstrating stronger statistical significance. These robust scaling relationships underscore that interparticle collisional stress governs the generation of fluctuating forces in rock-ice avalanches, where enhanced inertial interactions amplify force chain instabilities, dominating the spectral characteristics of basal force fluctuations.

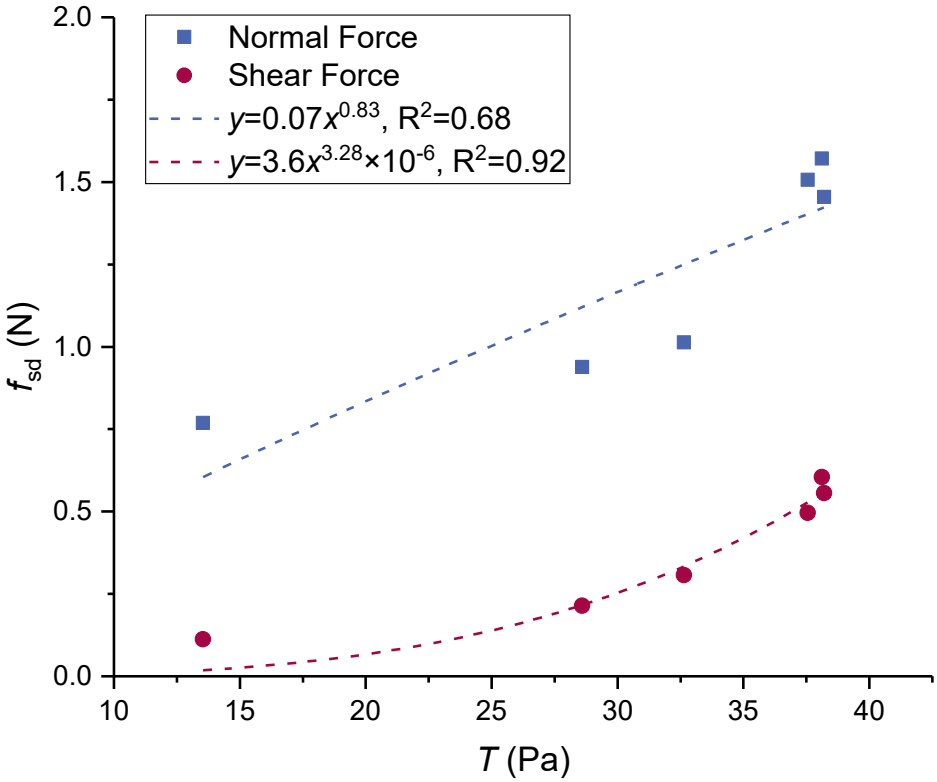

Figure 7. The relationship of the solid inertial stress (T) versus the standard deviations (f_{sd}) of the basal forces.

4. Conclusions

A series of DEM rotating drum simulations were used to investigate rock-ice avalanche flow behavior and dynamics, and we employed spherical particle approximations for ice and gravel phases, assuming homogeneous particle size distributions (i.e., uniform radii within each material type). These simulations, based on visual descriptions and basal force measurements, were used to examine basal force profiles and their statistical characteristics with varying ice content (φ_i), revealing the mechanical mechanisms behind force fluctuations through statistical analysis. The conclusions are summarized as follows:

(1) Phase segregation occurs in rock-ice binary granular flows within the rotating drum due to density and frictional disparities: low-density, low-friction ice particles migrate forward via buoyancy effects, while high-density gravels accumulate in the tail region through inertial settling and frictional dissipation.

(2) Ice content critically modulates avalanche basal dynamics. Higher φ_i reduces flow resistance by lowering interparticle friction and promoting ice segregation into surface layers, thus altering stress transmission. Basal force profiles transition from asymmetric to symmetric with increasing φ_i, while lower φ_i amplifies force fluctuations and extreme basal stress probabilities.

(3) Increasing φ_i linearly reduces mean basal force, extreme force, and force fluctuation intensity. The strong correlation between extreme force and fluctuation intensity suggests that basal stress variability originates from stochastic particle collisions, deviating from dry granular mechanics. Ice-mediated lubrication enhances collision-dominated momentum transfer while diminishing interparticle locking, driving a rheological transition in ice-rich flows.

(4) Basal stress fluctuations exhibit power-law dependencies on solid inertial stress (T), with basal forces showing stronger scaling. The scaling relationships confirm that collisional interactions govern fluctuating force generation, where increased inertial stress amplifies force chain instabilities and dictates basal dynamics spectral behavior.

Author contributions

Zhibo Dong: Conceptualization, Funding acquisition, Methodology, Writing–original draft. Zhiping Sun: Data curation, Writing–review & editing.

Use of AI tools declaration

The authors declare they have not used Artificial Intelligence (AI) tools in the creation of this article.

Acknowledgments

This work was supported by the Basic Scientific Research Projects of Higher Education Institutions in Liaoning Province (LJ212510154003), the Basic Scientific Research Fund of Liaoning Provincial Colleges and Universities (LJZZ222410154008) and the Liaoning Province Science and Technology Joint Plan Project (2024-BSLH-121).

Conflict of Interest

The authors declared that they do not have any commercial or associative interest that represents a conflict of interest in connection with the work submitted. Furthermore, there is no conflict of interest for the corresponding author and the co-authors.

References

1. Ren Y, Yang Q, Cheng Q, et al. (2021) Solid-liquid interaction caused by minor wetting in gravel-ice mixtures: A key factor for the mobility of rock-ice avalanches. *Eng Geol* 286: 106072. https://doi.org/10.1016/j.enggeo.2021.106072
2. Wang C, Cui Y, Song D, et al. (2022) Effect of ice content on the interaction between rock–ice avalanche and rigid barrier: Physical and numerical modelling. *Comput Geotech* 150: 104924. https://doi.org/10.1016/j.compgeo.2022.104924
3. Fan X, Yunus AP, Yang YH, et al. (2022) Imminent threat of rock-ice avalanches in High Mountain Asia. *Sci Total Environ* 836: 155380. https://doi.org/10.1016/j.scitotenv.2022.155380
4. Schneider D, Bartelt P, Caplan-Auerbach J, et al. (2010) Insights into rock-ice avalanche dynamics by combined analysis of seismic recordings and a numerical avalanche model. *J Geophys Res Earth Surf* 115: F04026. https://doi.org/10.1029/2010JF001734
5. Hu K, Zhang X, You Y, et al. (2019) Landslides and dammed lakes triggered by the 2017 Ms6.9 Milin earthquake in the Tsangpo gorge. *Landslides* 16: 993–1001. https://doi.org/10.1007/s10346-019-01168-w
6. Huggel C, Zgraggen-Oswald S, Haeberli W, et al. (2005) The 2002 rock/ice avalanche at Kolka/Karmadon, Russian Caucasus: assessment of extraordinary avalanche formation and mobility, and application of QuickBird satellite imagery. *Nat Hazards Earth Syst Sci* 5: 173–187. https://doi.org/10.5194/nhess-5-173-2005
7. Fujita K, Inoue H, Izumi T, et al. (2017) Anomalous winter-snow-amplified earthquake-induced disaster of the 2015 Langtang avalanche in Nepal. *Nat Hazards Earth Syst Sci* 17: 749–764. https://doi.org/10.5194/nhess-17-749-2017
8. Gardezi H, Xing A, Bilal M, et al. (2022) Preliminary investigation and dynamic analysis of a multiphase ice-rock avalanche on July 5, 2021, in the upper Naltar valley, Gilgit, Pakistan. *Landslides* 19: 451–463. https://doi.org/10.1007/s10346-021-01840-0
9. Cagnoli B, Romano GP (2012) Granular pressure at the base of dry flows of angular rock fragments as a function of grain size and flow volume: A relationship from laboratory experiments. *J Geophys Res Solid Earth* 117: B10202. https://doi.org/10.1029/2012JB009374
10. Wang YF, Cheng QG, Zhu Q (2015) Surface microscopic examination of quartz grains from rock avalanche basal facies. *Can Geotech J* 52: 167–181. https://doi.org/10.1139/cgj-2013-0284
11. Allstadt KE, Farin M, Iverson RM, et al. (2020) Measuring Basal Force Fluctuations of Debris Flows Using Seismic Recordings and Empirical Green's Functions. *J Geophys Res Earth Surf* 125: e2020JF005590. https://doi.org/10.1029/2020JF005590
12. Collins GS, Melosh HJ (2003) Acoustic fluidization and the extraordinary mobility of sturzstroms. *J Geophys Res Solid Earth* 108: 2473. https://doi.org/10.1029/2003JB002465
13. Iverson RM (1997) The physics of debris flows. *Rev Geophys* 35: 245–296. https://doi.org/10.1029/97RG00426

14. Li K, Wang Y, Cheng Q, et al. (2022) Insight Into Granular Flow Dynamics Relying on Basal Stress Measurements: From Experimental Flume Tests. *J Geophys Res Solid Earth* 127: e2021JB022905. https://doi.org/10.1029/2021JB022905
15. McArdell BW, Bartelt P, Kowalski J (2007) Field observations of basal forces and fluid pore pressure in a debris flow. *Geophys Res Lett* 34: L07406. https://doi.org/10.1029/2006GL029183
16. Schneider D, Kaitna R, Dietrich WE, et al. (2011) Frictional behavior of granular gravel-ice mixtures in vertically rotating drum experiments and implications for rock-ice avalanches. *Cold Reg Sci Technol* 69: 70–90. https://doi.org/10.1016/j.coldregions.2011.07.001
17. Dong Z, Su L (2023) Flow regimes and basal normal stresses in rock-ice avalanches by experimental rotating drum tests. *Cold Reg Sci Technol* 218: 104081. https://doi.org/10.1016/j.coldregions.2023.104081
18. Dong Z, Su L, Hu B, et al. (2024) Friction behaviors and flow resistances of rock-ice avalanches. *Cold Reg Sci Technol* 220: 104130. https://doi.org/10.1016/j.coldregions.2024.104130
19. Fan X, Feng Z, Ni T, et al. (2025) The Friction Behavior of Rock-Ice Avalanches in Relation to Rock-Ice Segregation: Insights From Flume Physical Experiments. *J Geophys Res Earth Surf* 130: e2024JF007904. https://doi.org/10.1029/2024JF007904
20. Feng Z, Fan X, Ni T, et al. (2023) How Ice Particles Increase Mobility of Rock-Ice Avalanches: Insights From Chute Flows Simulation of Granular Rock-Ice Mixtures by Discrete Element Method. *J Geophys Res Earth Surf* 128: e2023JF007115. https://doi.org/10.1029/2023JF007115
21. Zhou GGD, Cui KFE, Jing L, et al. (2024) Segregation-Induced Flow Transitions in Rock-Ice Mixtures: Implications for Rock-Ice Avalanche Dynamics. *J Geophys Res Earth Surf* 129: e2024JF007831. https://doi.org/10.1029/2024JF007831
22. Sun Z, Li S, Dong J, et al. (2025) Particle-density segregation of rock-ice avalanche. *AIP Adv* 15: 01521. https://doi.org/10.1063/5.0249871
23. Zhu Y, Jiang Y, Liu Y, et al. (2024) Material characteristic-controlled particle segregation in rock-ice avalanche. *Comput Geotech* 171: 106367. https://doi.org/10.1016/j.compgeo.2024.106367
24. Chou SH, Hu HJ, Hsiau SS (2016) Investigation of friction effect on granular dynamic behavior in a rotating drum. *Adv Powder Technol* 27: 1912–1921. https://doi.org/10.1016/j.apt.2016.06.022
25. Hsu L, Dietrich WE, Sklar LS (2014) Mean and fluctuating basal forces generated by granular flows: Laboratory observations in a large vertically rotating drum. *J Geophys Res Earth Surf* 119: 1283–1309. https://doi.org/10.1002/2013JF003078
26. McCoy SW, Tucker GE, Kean JW, et al. (2013) Field measurement of basal forces generated by erosive debris flows. *J Geophys Res Earth Surf* 118: 589–602. https://doi.org/10.1002/jgrf.20041
27. Yohannes B, Hsu L, Dietrich WE, et al. (2012) Boundary stresses due to impacts from dry granular flows. *J Geophys Res Earth Surf* 117: F02027. https://doi.org/10.1029/2011JF002150
28. Bagnold RA (1954) Experiments on a gravity-free dispersion of large solid spheres in a newtonian fluid under shear. *Proc R Soc Lond A* 225: 49–63. https://doi.org/10.1098/rspa.1954.0186
29. Iverson RM, Denlinger RP (2001) Flow of variably fluidized granular masses across three-dimensional terrain 1. Coulomb mixture theory. *J Geophys Res Solid Earth* 106: 537–552. https://doi.org/10.1029/2000JB900329
30. Xiao S, Su L, Jiang Y, et al. (2019) Estimating the maximum impact force of dry granular flow based on pileup characteristics. *J Mt Sci* 16: 2435–2452. https://doi.org/10.1007/s11629-019-5428-5

31. Jiang Y, Fan X, Li T, et al. (2018) Influence of particle-size segregation on the impact of dry granular flow. *Powder Technol* 340: 39–51. https://doi.org/10.1016/j.powtec.2018.09.014

Appendix: DEM theory

The discrete element simulations in this study were implemented using EDEM, a Computer-Aided Engineering (CAE) platform specialized in particulate system analysis. As a computational framework grounded in Newtonian mechanics, this software iteratively solves kinematic equations to track particle trajectories through temporal-spatial updates of displacement vectors and force equilibria. The contact mechanics governing interparticulate and boundary interactions were formulated through the Hertz-Mindlin constitutive model.

The no-slip variant of the Hertz-Mindlin model was adopted to characterize contact behavior between particulate assemblies and geometric boundaries [30,31]. This selection aligns with its established computational efficiency in handling non-cohesive granular systems. The normal force component (F_n) derives from the nonlinear Hertzian formulation dependent on normal overlap (δ_n), while the tangential force (F_t) incorporates tangential displacement (δ_t) and damping effects, as mathematically expressed in the constitutive equations:

$$F_n = \frac{4}{3} E^* \sqrt{R^*} d_n^{\frac{3}{2}} - 2 \times \sqrt{\frac{5}{6}} b \sqrt{S_n m^* v_n^{rel}} \tag{6}$$

$$F_t = -S_t \delta_t \tag{7}$$

where E^*, R^*, and m^* denote the normalized Young's modulus, scaled radius, and effective mass of a particle, respectively. These variables are mathematically expressed as:

$$\frac{1}{E^*} = \frac{1-\nu_i^2}{E_i} + \frac{1-\nu_j^2}{E_j} \tag{8}$$

$$\frac{1}{R^*} = \frac{1}{R_i} + \frac{1}{R_j} \tag{9}$$

$$\frac{1}{m^*} = \frac{1}{m_i} + \frac{1}{m_j} \tag{10}$$

where E, ν, R, and m represent Young's modulus, Poisson ratio, radius, and mass of particle, respectively. Subscripts i and j distinguish between interacting particles, while v_n^{rel} denotes their relative velocity. The normal stiffness S_n and tangential stiffness S_t are calculated via Equations 11 and 12, respectively, with the damping coefficient β derived from the restitution coefficient e (Equation 13):

$$S_n = 2E^* \sqrt{R^* \delta_n} \tag{11}$$

$$S_t = 8G^* \sqrt{R^* \delta_n} \tag{12}$$

$$\beta = \frac{-\ln e}{\sqrt{\ln^2 e + \pi^2}} \tag{13}$$

where G^* is the equivalent shear modulus, which can be given by the following formula:

$$G^* = \frac{E^*}{2(1+\nu)} \tag{14}$$

The rolling resistance moment M is applied to the surfaces of contact particles and can be given as follows:

$$M = \mu_r F_n R^* \tag{15}$$

where μ_r is the rolling friction coefficient.